Isolated Single-Atomic Cu Catalyst Supported on P-doped Carbon for Hydrochlorination of Acetylene

Ting Wang
Industrial Catalysis Institute of Zhejiang University of Technology
Zhao Jiang
Industrial Catalysis Institute of Zhejiang University of Technology
Qi Tang
Industrial Catalysis Institute of Zhejiang University of Technology
Bolin Wang
Industrial Catalysis Institute of Zhejiang University of Technology
Saisai Wang
Industrial Catalysis Institute of Zhejiang University of Technology
Mingde Yu
Industrial Catalysis Institute of Zhejiang University of Technology
Renqin Chang
Industrial Catalysis Institute of Zhejiang University of Technology
Yuxue Yue
Industrial Catalysis Institute of Zhejiang University of Technology
Jia Zhao (jiazhao@zjut.edu.cn)
Industrial Catalysis Institute of Zhejiang University of Technology
Xiaonian Li
Industrial Catalysis Institute of Zhejiang University of Technology

Article

Keywords: XPS, GHSV, HAADF-STEM, VCM, Langmuir-Hinshelwood, Cu-based catalysts

Posted Date: June 22nd, 2021

DOI: https://doi.org/10.21203/rs.3.rs-618887/v1

Version of Record: A version of this preprint was published at Communications Chemistry on January 10th, 2022. See the published version at https://doi.org/10.1038/s42004-021-00619-7.

Abstract

As an environmentally friendly non-mercury catalyst for the hydrochlorination of acetylene, Cu-based catalysts have always attracted attention. In this study, a series of phosphorus-doped Cu-based catalysts supported on activated carbon were prepared by the wet impregnation method, the difference of them is that the calcination temperature of phosphorus-doped carrier is 200 ℃, 400 ℃, 600 ℃ and 800 ℃ respectively. In the test conditions of T = 150℃, GHSV(C_2H_2) = 90 h^{-1} and V(HCl): V(C_2H_2) = 1.2, the highest acetylene conversion was 83.1%. The type of phosphorus configuration and the distribution on the surface of the carrier can be adjusted by changing the calcination temperature. Among the different phosphorus species formed by the phosphorus doping treatment at different temperatures, the P-C bond formed after the phosphorus element is incorporated into the carbon lattice also accounts for an increasing proportion with the increase of the calcination temperature,which is accompanied by a higher and higher acetylene conversion. It can be seen that the P-C bond plays a key role in the acetylene hydrochlorination reaction in this system. Meanwhile, Cu^{2+} was identified as the main active component in the catalyst by XPS. The representative HAADF-STEM image shows isolated copper species, confirming that the single-center copper species supported on the carbon support is the active center of the acetylene hydrochlorination reaction. The coordination structure formed by the interaction between the P-C bond and the atomically dispersed Cu^{2+} species is an effective and stable active site in the reaction. Density functional theory calculations indicate that the reaction is proposed to proceed according to the Langmuir-Hinshelwood (L-H) mechanism. This work is the first to identify which phosphorus species plays a role in the hydrochlorination of acetylene, which may provide some ideas for the design and optimization of phosphorus doping catalysts in the future.

1.introduction

The vinyl chloride monomer (VCM) used in the production of polyvinyl chloride (PVC) in China is mainly produced through the hydrochlorination of acetylene. At present, the development of low-cost and environmentally friendly non-precious metal catalysts is still attractive. Cu-based catalysts were widely studied at the beginning because of their high activity in vapor-phase hydrogenation reactions[1]. Similarly, the use of Cu-based catalysts in the hydrochlorination of acetylene has also been found to have good activity. Cu-based catalyst are now being widely investigated, but their conversion is lower than that of precious metal catalysts, and their activity and stability need to be enhanced due to the accumulation of metal active centers and the reduction of metal high valence states[2–8]. At present, its catalytic performance can be improved by means of carrier modification and addition of other metals.

It is known that the support can be modified by the doping of non-metallic elements such as nitrogen, boron and phosphorus on carbon materials to improve the catalytic performance of certain reactions[9–12]. In recent years, people are more and more interested in phosphorus-doped carbon materials. Chen *et al.*[13] found that electrocatalytic oxygen reduction reaction (ORR) activity can be improved because more structural defects are formed after the introduction of heteroatom phosphorus. Liu *et al.*[14–15] and

partners found that the prepared phosphorus-doped carbon nanotubes and graphite layers changed the electronic structure of the carbon material due to phosphorus doping, thus exhibiting high ORR performance and electrocatalytic activity. In order to be applied to acetylene hydrochlorination, there are also related studies have appeared. The support of the gold catalyst prepared by Wang *et al.*[16] was phosphorus-doped carbon with triphenylphosphine as the phosphorus source, which improves the conversion of acetylene and selectivity to vinyl chloride monomer[17–23]. Various characterization results show that the phosphorus group on the support can improve the dispersion of catalytic active sites, prevent the active gold species Au^{3+} and Au^{+} from reducing to Au^{0}, and can also delay the coking deposition on the catalyst surface[24–27]. Li *et al.*[2] prepared a phosphorus-doped copper catalyst supported on spherical activated carbon (SAC) with high activity and good stability. Phosphorus doping promotes the dispersion of copper species, enhances the interaction between metal and support, and inhibits agglomeration of copper species during the acetylene hydrochlorination process. Wang *et al.*[28–30] reported that the introduction of phosphorus can inhibit the reduction of Cu^{2+} during the reaction and promote the dispersion of active ingredients on the activated carbon support.

Although there have been many studies on phosphorus doping, it has not been investigated that which of the different phosphorus species produced during the preparation process can be the most suitable anchoring sites for metal coordination[31–36] to play a key role in acetylene hydrochlorination and how it interacts with copper species. In order to solve this problem, in this study, non-toxic and low-cost 1-hydroxyethylidene-1,1-diphosphonic acid (HEDP) is used as phosphorus source to prepare copper catalysts supported on phosphorus-doped activated carbon calcined at different temperatures. The proportion and distribution of phosphorus species on the surface of the carrier can be adjusted at different calcination temperatures. Combined with acetylene conversion and characterization analysis, we found that the P-C bond plays a crucial role in the hydrochlorination of acetylene, and the coordination structure formed by the interaction between atomically dispersed Cu^{2+} species and P-C bond is the reason for the better catalytic performance of the catalyst. Meanwhile, density functional theory (DFT) is used to further find that the reaction of C_2H_2 and HCl at the active site follows the L-H mechanism.

2. Experimental

2.1 Catalyst preparation

P-doped Cu-based catalysts supported on AC were synthesized by impregnation method with the solvent of deionized water. First, 3.325g HEDP was dissolved in 10 mL deionized water and stirred intensely until transparent and clear solution was achieved. 5g AC was slowly poured into the above liquid with stirring under room temperature, standing it for 4h. Then the obtained mixture was dried at 120°C for 12 h and calcined at 800°C for 1h under N_2 atmosphere at a heating rate of 10°C min^{-1} to synthesize carriers named PC800. Supports calcined at 200℃, 400℃ and 600℃ were prepared in the same way and named as PC200, PC400 and PC600, respectively. Subsequently, 1.05g $CuCl_2$ was dissolved in 10 mL deionized water and stirred until a blue homogeneous solution formed. Pretreated carbon PC800 was

added to a solution of $CuCl_2$ and maintained at room temperature for 4 h. Finally, the fresh catalyst was acquired after drying at 120°C for 12 h, denoted as Cu/PC800. By the same method, catalysts calcined at 200°C, 400°C and 600°C were prepared and named Cu/PC200, Cu/PC400 and Cu/PC600, respectively. In addition, the Cu/AC catalyst for comparison was synthesized by the impregnation method.

2.2 Catalyst characterization and computational details

Transmission electron microscopy (TEM) with a high-angle annular dark-field (HAADF) detector was acquired on a FEI Titan G2 60–300 microscope operating at 300kV, which can be conducted to detect morphologies of catalysts and to observe the distribution and size of Cu particles. Energy dispersive analysis of X-rays (EDX) was carried out on a Tecnai G2 F30 S transmission electron microscope operating at 300 keV. Nitrogen adsorption/desorption isotherms (BET) were acquired from a Micromeritics ASAP 2020 to test various structural parameters of the catalyst. X-ray diffraction (XRD) carried out on a PANalytical-X'Pert PRO generator with Cu Kα radiation was performed to determine dispersity and crystallinity of the active component and crystal form of the support. X-ray photoelectron spectroscopy (XPS) was conducted with a Kratos AXIS Ultra DLD spectrometer to distinguish chemical elements valence states of the catalyst surface. Raman spectroscopy was carried out in a WITec CRM 200 confocal Raman microscope. Fourier transform infrared spectroscopy (FT-IR) characterization was carried out on a Fourier transform infrared spectrophotometer (Nicolet 6700, Thermal Fisher Nicolet Corporation, Waltham, America). Temperature-programmed reduction (TPR) was conducted in a micro-flow reactor and recorded by a thermal conductivity detector (TCD) to investigate the reduced ability of the catalysts. Temperature-programmed desorption (TPD) was performed in a tubular quartz reactor and recorded by a thermal conductivity detector (TCD). All structures were optimized using gradient-corrected density functional theory (DFT) with the hybrid B3LYP exchange-correlation functional, which were performed using Gaussian 09 software package. A 6-31G(d) basis set was used for all atoms except for Cu, which has been described with Lanl2dz pseudo-potential basis set.

2.3 Catalytic test

A fixed-bed glass reactor was used to evaluate the performance of the catalysts. Two mL of the catalyst was added in the fixed position of the tubular reactor. The reactor was flushed with nitrogen for 30 min in order to remove water vapor and air. Then turn on the reaction heating, when the reactor temperature reached 150°C, N_2 was closed and purified hydrogen chloride (HCl) was fed into the tube reactor to activate catalyst for 30 min. Finally, a reaction gas mixture of acetylene (C_2H_2) and hydrogen chloride (HCl) was passed through the reactor at a gas hourly space velocity of C_2H_2 (GHSV) of $200h^{-1}$ with C_2H_2: HCl ratio of 1:1.2. The effluent streams of the reactor were passed through sodium hydroxide (NaOH) aqueous solution in an absorption bottle to separate any unreacted HCl from the gas products and was sent to be analyzed by an on-line gas chromatograph equipped with a flame ionization detector (FID) and a Porapak N packed column (6 ft × 1/800 stainless steel).

3.result And Discussion

3.1 Catalyst synthesis and characterization

Phosphorus is easily doped into the carbon framework during the calcination process after impregnation. The XPS and EDS results listed in the Table S1 and Fig. 1a show that there is a certain amount of phosphorus in this batch of catalysts, indicating that phosphorus is doped in the carbon framework.

In addition, nitrogen adsorption and desorption isotherms are used to measure P-doped activated carbons. The Table S2 lists the specific surface area and pore structure parameters of P-doped activated carbons calcined at different temperatures. The BET surface areas of Cu/PC200, Cu/PC400, Cu/PC600, and Cu/PC800 are 203, 420, 910, 1005 m^2g^{-1}, respectively. Compared with the specific surface area of activated carbon of 1204 m^2g^{-1}, both the specific surface area and pore volume of activated carbon after phosphorus doping treatment are smaller. The addition of phosphorus element may fill and block part of the pore of the carrier and occupy some available space. The larger specific surface area and pore volume of the catalysts calcined at 600℃ and 800℃ may be caused by the thermal decomposition of phosphorus ligand at high temperature and the reduction of blocked pores. The pore size of phosphorus-doped activated carbon is similar, and it is also relatively close to activated carbon. Previous reports generally agree that a higher specific surface area can expose more active sites to promote the transfer of the substrate, which is conducive to improving the activity. The results of this study are also the same. The carbon carrier calcined at 800°C has the largest specific surface area, and the corresponding acetylene conversion rate is also the highest among several catalysts. As shown in the Fig. 1b, the N_2 adsorption-desorption isotherm of PC800 with the best effect is a typical IV type curve with obvious hysteresis loop characteristics of mesoporous structure, indicating that the PC800 carrier has a multi-stage pore structure and other catalysts also have hysteresis loop characteristics. The Fig. S1a,b,c shows that several other catalysts also have hysteresis loop characteristics.

Figure 1c shows the XRD patterns of each fresh Cu-based catalyst. The amorphous diffraction peaks of the carbon carrier at 25° and 43° correspond to the plane of (002) and (101), respectively[37]. In addition, no other discernible diffraction peaks are detected in the Cu-based catalyst, which means that the copper particle size is below the detection limit of the XRD instrument, or the copper species on the activated carbon support is in an amorphous form[38–39]. It can be speculated that the copper species can be well dispersed on the P-doped carbon support, and the presence of phosphorus can enhance the dispersibility of copper active sites.

The Fig. S2 shows the morphology of each phosphorus-doped catalyst, showing a classic two-dimensional (2D) carbon nanosheet structure, with obvious wrinkles which may be caused by phosphorus doping. The size of phosphorus atoms is larger than carbon atoms, resulting in local geometric distortion in the carbon skeleton. Meanwhile, there are almost no copper nanoparticles in these fresh catalysts, indicating that the introduction of phosphorus atoms can make the copper species well dispersed on the support. The presence of phosphorus atoms on the carrier may provide new active sites, and the coordination structure formed with copper species may be the main active sites. These results are consistent with the previous XRD spectra analysis.

In addition, further analysis of HAADF-STEM image (Fig. 1d and Fig. S3a,c,e) reveals the existence of highly dispersed isolated copper species, and no copper nanoparticles are found. It's confirmed that the single center copper species supported on carbon support is the active center of acetylene hydrochlorination reaction, indicating that the active component of the catalyst is composed of atom dispersed copper[40–42]. The element mapping of the catalyst Cu/PC800 (Fig. 1e) reveals that C, P and Cu elements are uniformly distributed on the surface of the catalyst, which is also consistent with the previous XPS results, verifying the successful doping of phosphorus in the carbon support, as well as the other catalysts (Fig. S3b,d,f).

Figure2.(a) The conversion of acetylene over P-doped Cu-based catalysts. Reaction conditions: temperature=150℃, GHSV(C_2H_2)=90 h^{-1}, V(HCl)/V(C_2H_2)=1.2/1, (b)Comparison of acetylene conversions for Cu/PC200, Cu/PC400, Cu/PC600 and Cu/PC800 catalysts and their respective treated carbons,(c) Kinetic studies of Cu/AC and Cu/PC800 catalyst: apparent activation energy, kJ mol^{-1}, (d) GHSV plotted against the TOF for some copper-based catalysts reported in literature and Cu/PC800 catalyst with better catalytic performance in this article.

3.2 Catalytic performance of Cu-based catalysts

The catalyst shown in the Fig. 2a has the same copper load and phosphorus doping amount in the preparation process. Under the test conditions of T = 150℃, GHSV(C_2H_2) = 90 h^{-1} and V(HCl): V(C_2H_2) = 1.2, the initial conversion of acetylene is significantly different due to the different calcination temperatures of phosphorous doped carbon carriers. The initial conversion of acetylene increases with the increase of calcination temperature. These catalysts don't deactivate within 10 h, and Cu/PC800 shows a better catalytic performance with the highest conversion reaching 83.1%. As we can see, the Fig. S4 clearly shows that the VCM selectivity of all catalysts has reached more than 99%. Obviously, all the P-doped Cu-based catalysts in the Fig. 2b show a higher initial conversion than pure Cu/AC (the initial conversion is 35.46%). However, the activity of several phosphorus-doped carbon supports without the active component copper is very low, indicating that the enhanced activity of the copper-based catalyst is due to the interaction and synergistic effect between the active copper species and the phosphorus-doped activated carbon, rather than simply the sum of the parts.

In addition, through experiments at different temperatures, the Arrhenius equation is used to plot and the experimental activation energy (Ea) is obtained through linear fitting (Fig. 2c). At this time, the internal and external diffusion of the reaction have been eliminated, and the reaction is under kinetic control. The apparent activation energy of the Cu/PC800 catalyst with the best catalytic performance in the figure is calculated to be 23 kJ mol^{-1}. The activation energy of the classic Cu-based catalyst Cu/AC is 34 kJ mol^{-1}, and the calculated result of the P-doped Cu-based catalyst is lower than this value, indicating that acetylene is more likely to react with hydrogen chloride on the P-doped Cu-based catalyst than the classic copper catalyst. In order to demonstrate the excellent performance of P-doped Cu-based catalysts, the Cu/PC800 catalyst is compared with some copper-based catalysts published in literature (note that the experimental conditions are not necessarily the same). The turnover frequency (TOF) at the beginning of

the experiment is plotted versus GHSV, and is shown in Fig. 2d. Various copper catalysts from the literature[3,7,43–51] is used for this comparison, and it is obvious that the Cu/PC800 catalyst is one of the better catalysts that can provide higher yields of vinyl chloride at relatively high space velocities (colored areas in the figure) compared to some of the catalysts reported.

3.3 Identification of the catalytic active sites

The Fig. 3a shows the XRD pattern of the used sample, which is similar to the fresh catalyst. The two main diffraction peaks at approximately 25° and 43° correspond to the (002) and (101) crystal planes of carbon, respectively[52–56]. Except for the two diffraction peaks, no other characteristic peaks were found. The active copper species on the phosphorus-doped carbon support was always dispersed very well during the reaction.

As shown in Fig. 3b, Raman spectroscopy shows that all samples have two characteristic peaks near 1350 and 1590 cm^{-1}, which are attributed to the absorption peaks of the D band and G band in the carbon material respectively. The G band is generated by the vibration of sp2 hybridized graphite-type carbon atoms, indicating the degree of graphitization of carbon materials, while the D band is usually caused by sp3 hybridized carbon atoms and structural defects, indicating the disordered structure and defect. The doping of phosphorus atoms destroys the hexagonal symmetry of the graphene plane[57], which increases the number of defect sites in the activated carbon framework. The higher the temperature, the lower the regularity and order of the sample.

XPS spectroscopy can be used to analyze the chemical state of copper on the catalyst surface, and the relative content of different copper species can be calculated according to the relative deconvolution peak area. The Fig. 3d shows that in each P-doped Cu-based catalyst, the main peak with a binding energy of about 934.5 eV belongs to Cu^{2+}, and the peak with a binding energy of about 932.3 eV belongs to Cu^{+} and Cu^{0} [39,49]. The XAES spectrum can be used to distinguish Cu^{+} from Cu^{0}. In the XAES spectrum shown in the Fig. 3e, the peak of Cu^{+} can be observed at 916.6eV, and the peak of Cu^{0} can be observed at about 918.6eV[7,30]. The Table S3 and Fig. S5a lists the binding energy positions and the relative content of different copper species Cu^{2+}, Cu^{+} and Cu^{0}. It can be found that Cu^{2+} and Cu^{+} are both active components for P-doped Cu-based catalysts, but with the increase of calcination temperature, the proportion of Cu^{2+} increases significantly, and the amount of Cu^{+} and Cu^{0} decreases, combined with the result of the acetylene conversion (Fig. 4a-c), the catalytic activity is the best when calcination temperature is 800 ℃, so the presence of Cu^{2+} is more conducive to the improvement of catalyst activity.

The P 2p spectrum shown in the Fig. 3f can be deconvolved into three peaks to determine the relative content and species of phosphorus. The peaks with binding energies around 135.1eV, 134.2eV and 133.0eV correspond to three different phosphorus species, P = O, P-O and P-C respectively[53–56], which is also confirmed by FT-IR (Fig. 3c). The P-O bond represents all phosphorus-containing functional groups related to oxygen. The P-C bond indicates that the phosphorus atom is indeed successfully incorporated into the carbon lattice. The binding energy and the relative amount of each phosphorus species in the p-

doped Cu-based catalysts are listed in the Table S4. Although the P-O bond occupies the highest proportion in each catalyst, only the relative contents of the P-C bond increase significantly with the increase of roasting temperature, while the relative contents of the P = O bond and the P-O bond decrease. Combined with the catalytic activity of Cu-based catalysts (Fig. 4d-f), the P-C bond has the largest proportion (41.6%) in the catalysts calcined at 800℃, indicating that the higher the content of P-C bond, the more phosphorus atoms entering the carbon skeleton, the more favorable the catalyst to obtain higher catalytic activity.

In order to further analyze the chemical bond configuration of phosphorus in the catalyst, the O 1s peak is deconvolved into two components. As shown in the Fig. S5b, the peak at about 531.4 eV of all catalysts is attributed to non-bridging oxygen (P = O) [50,58], and the peak at about 532.6eV of binding energy is attributed to P-O-Cu bond and accounts for a large proportion[54], which is consistent with the result of P 2p spectrum. It further indicates that P-O-Cu bond is included in the oxygen related phosphorus-containing functional group represented by P-O bond, and the coordination structure of Cu and O in P-O bond is relatively stable. In addition, combined with the results of the Table S5 and the acetylene conversion (Fig. S6), as the calcination temperature increases, the relative content of P = O bond decreases slightly, and the relative content of P-O-Cu bond increases slightly, but the change range of both is very small, indicating that the variation of calcination temperature has little effect on the proportion of P = O bond and P-O-Cu bond and they have no significant positive effect on the activity of the catalyst, which can also be verified by the P 2p spectra. It should be noted that although the oxygen related phosphorus-containing functional groups represented by the P-O bond will decrease with the increase of the calcination temperature, the change of P-O-Cu bond contained in it is negligible. In general, the distribution of phosphorus species on the surface of the support can be adjusted by changing the roasting temperature. For the P-doped Cu-based catalyst in this study, the increase of the calcination temperature only leads to a significant increase in the relative content of P-C bond, which has a positive impact on the catalytic activity. Combined with the results of P 2p spectra, it can be inferred that Cu^{2+} and P-C bond can play a positive role in the hydrochlorination of acetylene, and the coordination structure formed by their interaction is the main active site of the Cu-based catalyst.

It has been reported that experimentally, many phosphorus doping methods, including high-temperature firing in an inert environment, are often accompanied by oxygen doping, so that different types of phosphorus and oxygen-containing functional groups can be formed[59–60]. Referring to the XPS results, P-O bonds, P = O bonds and P-C bonds may constitute various phosphorus and oxygen-containing groups and the bonding configuration of phosphorus entering the carbon matrix (Fig. 5c).

The TPR curves of each catalyst are shown in the Fig. 5a. Two main reduction peaks can be detected in all catalysts. The first hydrogen consumption peak appears in the range of 230°C to 330°C, and the second peak appears in the temperature range of 470°C to 570°C, these two reduction peaks are attributed to the reduction of Cu^{2+} species to Cu^{+} species and the change of Cu^{+} species to metallic copper, respectively [61]. The reduction peaks of Cu^{2+} and Cu^{+} move to higher temperatures with the

increase of the calcination temperature of the phosphorus-doped carbon support. The temperatures of the two reduction peaks of Cu/PC800 have increased to different degrees compared with other catalysts. It shows that compared with other catalysts calcined at other temperatures, there is a stronger interaction between copper and phosphorus-doped carbon support in Cu/PC800 catalyst, which effectively improves the anti-reduction ability of Cu^{2+} and Cu^{+} species. In addition, the reduction peak area of Cu^{2+} in the Cu/PC800 catalyst is significantly larger than other catalysts, indicating that the coordination structure formed by Cu and P atoms stabilizes the high-valent copper, and to a certain extent delays the reduction of the oxidation state Cu^{2+} species during the preparation process. This is the same as the result of XPS spectra. The relatively excellent catalytic performance of Cu/PC800 catalyst comes from the interaction between the Cu^{2+} species with high valence and the P-C bond.

TPD characterization can analyze the adsorption of the catalyst to the reactants, but the phosphorus ligand will be thermally decomposed at a higher temperature. In order to avoid interference to the acetylene signal from the sample desorption, TPD-MS experiment is used to study the adsorption of acetylene by the active site of the catalyst. The results are shown in Fig. 5b. Each catalyst has two desorption peaks, indicating that there are two active sites capable of adsorbing substrates, which may be Cu^{2+} active centers and Cu^{+} active centers, respectively. It has been reported that in the Cu(Ⅱ)/AC catalyst, the adsorption energy of acetylene on the copper center is less than that of the Cu(Ⅰ)/AC catalyst, and the smaller adsorption energy is usually desorbed first[49]. Therefore, the desorption peak at lower temperature and the desorption peak at higher temperature are likely to be attributed to the active center of Cu^{2+} and Cu^{+} respectively. The Cu^{2+} active species is the main active center. By comparing the different catalysts, it can be found that with the increase of calcination temperature, the peak area and desorption temperature of the desorption peak related to Cu^{2+} increase, especially for the catalyst with the calcination temperature of 800℃. The peak area of desorption peak is widely considered to represent the adsorption capacity. The larger the area is, the more active sites exist and the more acetylene is adsorbed on the corresponding active sites. The desorption temperature represents the strength of adsorption, and a high temperature indicates a stronger adsorption capacity for acetylene. Therefore, more Cu^{2+} active sites are conducive to the improvement of the catalytic performance of our series of phosphorus-doped copper-based catalysts, and the strong adsorption of related active sites on acetylene is beneficial to improve the activity and stability of the catalyst. Some results of TPD-MS are the same as those of XPS and TPR above.

To understand the activity of Cu^{2+} active sites loaded on phosphorus-doped carbon support, considering five phosphorus species (C_3P, P = O, $(OH)_2P$=O, $P(OH)_2$, (OH)P = O) mentioned in Fig. 4d-f, we carry out a series of theoretical studies aimed at exploring the underlying reaction mechanism. When encountering computational modelling for the active center, we have taken our computing power and time efficiency into full consideration, so we adopt a simple monolayer carbonic cluster saturated by hydrogen atoms ($C_{13}H_9$) in Fig. S7a to simulate carbon support[12]. The overall calculated results are shown in Fig. 6 and Fig. S7.

The adsorption energy of C_2H_2 on five different phosphorus species active sites are − 31.77, -42.27, -85.07, -21.26, -16.54kJ/mol respectively (Fig. S7b-f). It is obvious that $P(OH)_2$ and (OH)P = O copper active sites show weak interaction with C_2H_2. The P = O active site shows better adsorption to C_2H_2, but O of P = O bond may interact strongly with the Cl of HCl, which may cause complex reaction mechanism. Here we do not discuss the P = O species. The $(OH)_2P=O$ would decompose at our reaction temperature. Then only the C_3P specie was left.

The optimized structure of Cu^{2+} species adsorbed on the C_3P carbon support exist strong interaction between P and Cl, which may be real reason for the activity of our P-doped Cu-based catalyst. After C_2H_2 and HCl adsorbed on the active site, the C ≡ C bond length and H-Cl bond length is 1.2254Å and 1.3354Å respectively (Fig. 6a, d), which is 1.2012Å and 1.2895Å in the gas phase in reference. As is shown in the Fig. 6b-c, the molecular orbital of C_2H_2-complex displays interaction between C_2H_2 and Cu^{2+} active sites, and there is an orbital overlap between the Cu atom d orbital and the acetylene π^* orbital, while the molecular orbital of HCl-complex is different between HCl and active sites. However, the adsorption energy of C_2H_2 and HCl on Cu^{2+} species are calculated at -31.77 and − 34.13 kJ/mol. With cooperation of the nearly equal adsorption energy, it renders that the Cu^{2+} species after loaded to the P-doped carbon support can active both C_2H_2 and HCl of the same class. Subsequently, the adsorption of C_2H_2 and HCl at the active site may cause acetylene hydrochlorination reaction following the L-H mechanism shown in Fig. 6e. C_2H_2 and HCl co-adsorbed species (C_2H_2* and HCl*) reacted with each other to produce vinyl chloride.

4. Conclusions

We synthesized copper-based catalysts supported on phosphorous-doped carbon carriers calcined at different temperatures. The type and distribution of phosphorus configurations on the support can be adjusted by different calcination temperatures. Combined with the characterization, it was found that with the increase of calcination temperature, the proportion of P-C bond formed after phosphorus atoms entered the carbon lattice in the catalyst increased, and the acetylene conversion also increased. The XPS results of Cu showed that the activity of the catalyst was attributed to the presence of Cu^{2+} species, and no copper nanoparticles were found in HAADF-STEM images. The presence of isolated copper species confirmed that the single-site copper species supported on the phosphorus-doped carbon carrier was the active center of acetylene hydrochlorination reaction. In summary, it can be seen that P-C bond played a key role in the acetylene hydrochlorination reaction in this system, and the coordination structure formed by P-C bond and atomically dispersed Cu^{2+} species was the effective active site leading to better performance of the catalyst. Combined with the calculation of density functional theory, it can be observed that the catalyst of this system follows the Langmuir-Hinshelwood (L-H) mechanism in the acetylene hydrochlorination reaction. This work is the first to identify which phosphorus species plays a role in the hydrochlorination of acetylene, which may provide some ideas for the design and optimization of phosphorus doping catalysts in the future.

Declarations

Acknowledgements

Financial support from the National Natural Science Foundation of China (NSFC; grant No. 21606199), the Science and Technology Department of Zhejiang Province

References

1. Kobayashi, H., Takezawa, N. & Minochi, C. Methanol-reforming reaction over copper-containing catalysts—The effects of anions and copper loading in the preparation of the catalysts by kneading method. *J. Catal.* **69**, 487–494 (1981).
2. Ren, Y. et al. Chlorocuprate(â) ionic liquid as an efficient and stable Cu-based catalyst for hydrochlorination of acetylene. *Catal. Sci. Technol.* **9**, 2868–2878 (2019).
3. Zhao, W., Zhu, M. & Dai, B. The preparation of Cu-g-C_3N_4/AC catalyst for acetylene hydrochlorination. *J. Catal.* **6**, 193–203 (2016).
4. Ma, J., Wang, S. & Shen, B. Study on the effects of acetylene on an Au-Cu/C catalyst for acetylene hydrochlorination using Monte Carlo and DFT methods. *React. Kinet. Mech. Cat.* **110**, 177–186 (2013).
5. Zhang, X. et al. Highly dispersed copper over β–Mo_2C as an efficient and stable catalyst for the reverse water gas shift (RWGS) reaction. *ACS Catal.* **7**, 912–918 (2017).
6. Sagar, G. V., Rao, P. V., Srikanth, C. S. & Chary, K. V. R. Dispersion and reactivity of copper catalysts supported on Al_2O_3-ZrO_2. *J. Phys. Chem. B* **110**, 13881–13888 (2006).
7. Li, H., Wang, F., Cai, W., Zhang, J. & Zhang, X. Hydrochlorination of acetylene using supported phosphorus-doped Cu-based catalysts. *Catal. Sci. Technol.* **5**, 5174–5184 (2015).
8. Li, R. et al. Selective hydrogenation of acetylene over Pd-Sn catalyst: Identification of Pd_2Sn intermetallic alloy and crystal plane-dependent performance. *Appl. Catal. B Environ.* **279**, 119348–119358 (2020).
9. Zhao, J. et al. Supported ionic liquid-palladium catalyst for the highly effective hydrochlorination of acetylene. *Chem. Eng. J.* **360**, 38–46 (2019).
10. Li, R., Wei, Z., Gou, X. & Xu, W. Phosphorus-doped graphene nanosheets as efficient metal-free oxygen reduction electrocatalysts. *RSC Adv.* **3**, 9978–9984 (2013).
11. Wu, J. et al. Phosphorus-doped porous carbons as efficient electrocatalysts for oxygen reduction. *J. Mater. Chem. A* **1**, 9889–9896 (2013).
12. Wang, X., Dai, B., Wang, Y. & Yu, F. Nitrogen-doped pitch-based spherical active carbon as a nonmetal catalyst for acetylene hydrochlorination. *ChemCatChem* **6**, 2339–2344 (2014).
13. Chen, Z., Higgins, D., Tao, H., Hsu, R. S. & Chen, Z. Highly active nitrogen-doped carbon nanotubes for oxygen reduction reaction in fuel cell applications. *J. Phys. Chem. C* **113**, 21008–21013 (2009).

14. Liu, Z. et al. Novel phosphorus-doped multiwalled nanotubes with high electrocatalytic activity for O_2 reduction in alkaline medium. *Catal. Commun.* **16**, 35–38 (2011).
15. Liu, Z. et al. Phosphorus-doped graphite layers with high electrocatalytic activity for the O_2 reduction in an alkaline medium. *Angew. Chem. Int. Edit.* **50**, 3257–3261 (2011).
16. Wang, B. et al. Phosphorus-doped carbon supports enhance gold-based catalysts for acetylene hydrochlorination. *RSC Adv.* **4**, 15877–15885 (2014).
17. Zhou, K. et al. Synergistic gold-bismuth catalysis for non-mercury hydrochlorination of acetylene to vinyl chloride monomer. *ACS Catal.* **4**, 3112–3116 (2014).
18. Zhao, J. et al. Alternative solvent to aqua regia to activate Au/AC catalysts for the hydrochlorination of acetylene. *J. Catal.* **350**, 149–158 (2017).
19. Conte, M. et al. Characterization of Au^{3+} species in Au/C catalysts for the hydrochlorination reaction of acetylene. *Catal. Lett.* **144**, 1–8 (2013).
20. Conte, M. et al. Aqua regia activated Au/C catalysts for the hydrochlorination of acetylene. *J. Catal.* **297**, 128–136 (2013).
21. Zhao, J. et al. Towards a greener approach for the preparation of highly active gold/carbon catalyst for the hydrochlorination of ethyne. *J. Catal.* **365**, 153–162 (2018).
22. Zhao, J. et al. Stabilizing Au (III) in supported-ionic-liquid-phase (SILP) catalyst using $CuCl_2$ via a redox mechanism. *Appl. Catal. B Environ.* **206**, 175–183 (2017).
23. Hutchings, G. J. Au catalysts for acetylene hydrochlorination and carbon monoxide oxidation. *Top. Catal.* **57**, 1265–1271 (2014).
24. Zhao, J. et al. Supported ionic-liquid-phase-stabilized Au (III) catalyst for acetylene hydrochlorination. *Catal. Sci. Technol.* **6**, 3263–3270 (2016).
25. Liu, X. et al. Investigation of the active species in the carbon-supported gold catalyst for acetylene hydrochlorination. *Catal. Sci. Technol.* **6**, 5144–5153 (2016).
26. Zhao, J. et al. Enhancement of Au/AC acetylene hydrochlorination catalyst activity and stability via nitrogen-modified activated carbon support. *Chem. Eng. J.* **262**, 1152–1160 (2015).
27. Zhao, J. et al. Acetylene hydrochlorination over supported ionic liquid phase (SILP) gold-based catalyst: stabilization of cationic Au species via chemical activation of hydrogen chloride and corresponding mechanisms. *Chinese J. Catal.* **42**, 334–346 (2021).
28. Wang, B. et al. Stabilizing supported gold catalysts in acetylene hydrochlorination by constructing an acetylene-deficient reaction phase. *Green Energy Environ.* **6**, 9–14 (2021).
29. Conte, M., Carley, A. F. & Hutchings, G. J. Reactivation of a carbon-supported gold catalyst for the hydrochlorination of acetylene. *Catal. Lett.* **124**, 165–167 (2008).
30. Wang, X., Zhu, M. & Dai, B. Effect of phosphorus ligand on Cu-based catalysts for acetylene hydrochlorination. *ACS Sustain. Chem. Eng.* **7**, 6170–6177 (2019).
31. Wang, X. et al. Carbon-supported ruthenium catalysts prepared by a coordination strategy for acetylene hydrochlorination. *Chinese J. Catal.* **41**, 1683–1691 (2020).

32. Vilé, G. et al. A stable single-site palladium catalyst for hydrogenations. *Angew. Chem. Int. Edit.* **54**, 11265–11269 (2015).
33. Chen, Z. et al. Coordination-controlled single atom tungsten as a non-3d-metal oxygen reduction reaction electrocatalyst with ultrahigh mass activity. *Nano Energy* **60**, 394–403 (2019).
34. Qian, H. et al. Non-catalytic CVD preparation of carbon spheres with a specific size. *Carbon* **42**, 761–766 (2004).
35. Zhang, H. et al. Ru-Co (III)-Cu (II)/SAC catalyst for acetylene hydrochlorination. *Appl. Catal. B En*viron. **189**, 56–64 (2016).
36. Zhao, J. et al. Supported ionic liquid-palladium catalyst for the highly effective hydrochlorination of acetylene. *Chem. Eng. J.* **360**, 38–46 (2019).
37. Zhao, J. et al. Nitrogen- and phosphorus-codoped carbon-based catalyst for acetylene hydrochlorination. *J. Catal.* **373**, 240–249 (2019).
38. Patel, M. A. et al. P-doped porous carbon as metal free catalysts for selective aerobic oxidation with an unexpected mechanism. *ACS Nano* **10**, 2305–2315 (2016).
39. Severino, F., Brito, J. L., Laine, J., Fierro, J. L. G. & Agudo, A. L. Nature of copper active sites in the carbon monoxide oxidation on $CuAl_2O_4$ and $CuCr_2O_4$ spinel type catalysts. *J. Catal.* **177**, 82–95 (1998).
40. Hashmi, A. S. K. & Hutchings, G. J. Gold catalysis. *Angew. Chem. Int. Edit.* **45**, 7896–7936 (2006).
41. Hutchings, G. J. & Kiely, C. J. Strategies for the synthesis of supported gold palladium nanoparticles with controlled morphology and composition. *Accounts. Chem. Res.* **46**, 1759–1772 (2013).
42. Tang, Z. et al. Nanocrystalline cerium oxide produced by supercritical antisolvent precipitation as a support for high-activity gold catalysts. *J. Catal.* **249**, 208–219 (2007).
43. Qin, G. et al. Gas-liquid acetylene hydrochlorination under nonmercuric catalysis using ionic liquids as reaction media. *Green Chem.* **13**, 1495–1498 (2011).
44. Zhou, K. et al. Reactivity enhancement of N-CNTs in green catalysis of C_2H_2 hydrochlorination by a Cu catalyst. *RSC Adv.* **4**, 7766–7769 (2014).
45. Han, W. et al. Melamine modification of spherical activated carbon and its effects on acetylene hydrochlorination. *J. Wuhan Univ. Technol.* **29**, 1147–1151 (2014).
46. Xu, H., Si, J. & Luo, G. The kinetics model and fixed bed reactor simulation of Cu catalyst for acetylene hydrochlorination. *Int. J. Chem. React. Eng.* **15**, 20160165 (2017).
47. Wang, X., Zhu, M. & Dai, B. Effect of phosphorus ligand on Cu-based catalysts for acetylene hydrochlorination. *ACS Sustain. Chem. Eng.* **7**, 6170–6177 (2019).
48. Wang, Y., Nian, Y., Zhang, J., Li, W. & Han, Y. MOMTPPC improved Cu-based heterogeneous catalyst with high efficiency for acetylene hydrochlorination. *Mole. Catal.* **479**, 110612 (2019).
49. Zhao, C., Zhang, X., He, Z., Guan, Q. & Li, W. Demystifying the mechanism of NMP ligands in promoting Cu-catalyzed acetylene hydrochlorination: insights from a density functional theory study. *Inorg. Chem. Front.* **7**, 3204–3216 (2020).

50. Hu, Y. et al. High performance of supported Cu-based catalysts modulated via phosphamide coordination in acetylene hydrochlorination. *Appl. Catal. A Gen.* **591**, 117408 (2020).
51. Han, Y. et al. Pyrrolidone ligand improved Cu-based catalysts with high performance for acetylene hydrochlorination. *Appl. Organomet. Chem.* **35**, e6066 (2020).
52. Chang, F., Yang, H., Roselin, L. S. & Kuo, W. Ethanol dehydrogenation over copper catalysts on rice husk ash prepared by ion exchange. *Appl. Catal. A Gen.* **304**, 30–39 (2006).
53. Guo, Y. et al. Co_2P-CoN double active centers confined in N-doped carbon nanotube: heterostructural engineering for trifunctional catalysis toward HER, ORR, OER, and Zn-air batteries driven water splitting. *Adv. Funct. Mater.* **28**, 1805641 (2018).
54. Wu, J. et al. An efficient cobalt phosphide electrocatalyst derived from cobalt phosphonate complex for all-pH hydrogen evolution reaction and overall water splitting in alkaline solution. *Small* **16**, 1900550 (2019).
55. Raskar, D., Rinke, M. T. & Eckert, H. The mixed-network former effect in phosphate glasses: NMR and XPS studies of the connectivity distribution in the glass system $(NaPO_3)_{1-x}(B_2O_3)_x$. *J. Phys. Chem. C* **112**, 12530–12539 (2008).
56. Zhao, C., Gao, Y., Zhang, Z. & Ma, D. Functions of phytic acid in fabricating metal-free carbon catalyst for the oxidative coupling of benzylamines. *Chinese J. Chem.* **38**, 1292–1298 (2020).
57. Polster, C. S., Nair, H. & Baertsch, C. D. Study of active sites and mechanism responsible for highly selective CO oxidation in H_2 rich atmospheres on a mixed Cu and Ce oxide catalyst. *J. Catal.* **266**, 308–319 (2009).
58. Liu, W. et al. Phosphorus-doped graphite layers with high electrocatalytic activity for the O_2 reduction in an alkaline medium. *Angew. Chem. Int. Edit.* **50**, 3257–3261 (2011).
59. Latorre-Sánchez, M., Primo, A. & Garcia, H. P-doped graphene obtained by pyrolysis of modified alginate as a photocatalyst for hydrogen generation from water-methanol mixtures. *Angew. Chem. Int. Edit.* **52**, 11813–11816 (2013).
60. Liu, Z. et al. Preparation of phosphorus-doped carbon nanospheres and their electrocatalytic performance for O_2 reduction. *J. Nat. Gas. Chem.* **21**, 257–264 (2012).
61. Wang, B. et al. Hydrochlorination of acetylene on single-atom Pd/N-doped carbon catalysts: Importance of pyridinic-N synergism. *Appl. Catal. B Environ.* **272**, 118944–118954 (2020).

Figures

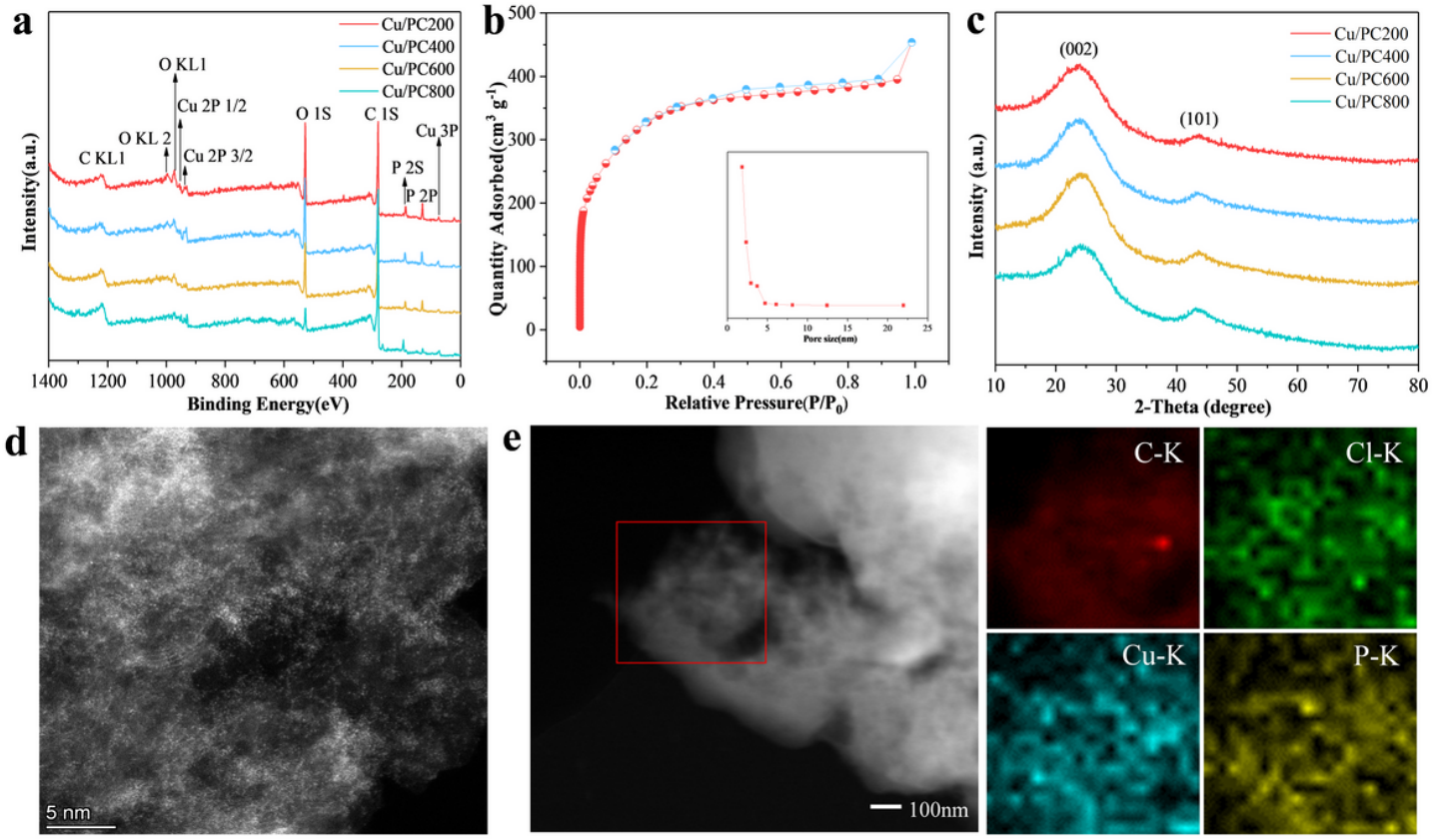

Figure 1

Characterizations of catalyst materials: (a) full XPS spectra of fresh P-doped Cu-based catalysts, (b) N2 gas adsorption/desorption isotherms of PC800, (c) XRD pattern of fresh P-doped Cu-based catalysts, (d) Representative HAADF-STEM images of fresh Cu/PC800 catalysts. Representative HAADF-STEM image showing isolated Cu species, (e) EDS elemental mapping of fresh Cu/PC800.

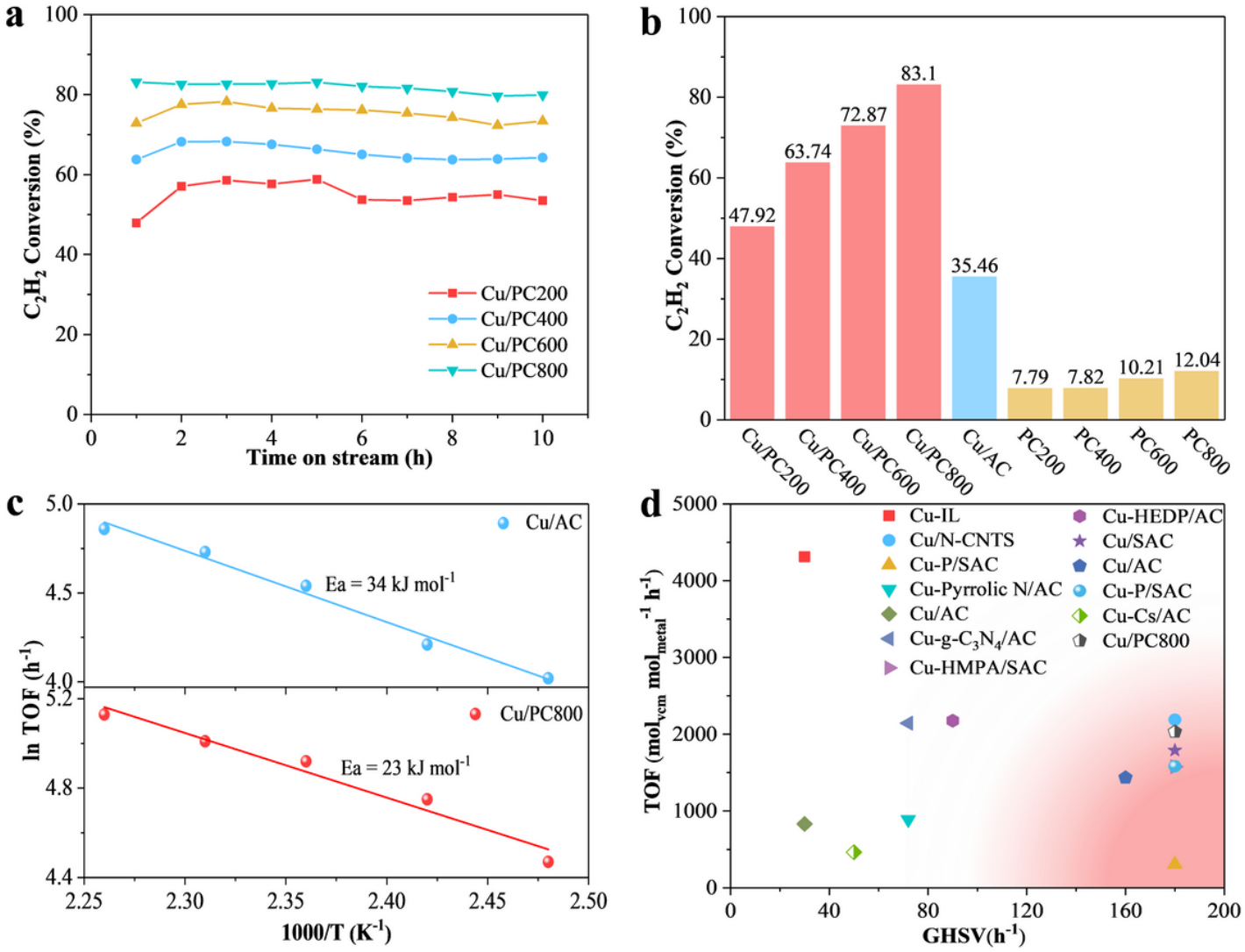

Figure 2

(a) The conversion of acetylene over P-doped Cu-based catalysts. Reaction conditions: temperature = 150°C, GHSV(C2H2) = 90 h-1, V(HCl)/V(C2H2) = 1.2/1, (b) Comparison of acetylene conversions for Cu/PC200, Cu/PC400, Cu/PC600 and Cu/PC800 catalysts and their respective treated carbons, (c) Kinetic studies of Cu/AC and Cu/PC800 catalyst: apparent activation energy, kJ mol-1, (d) GHSV plotted against the TOF for some copper-based catalysts reported in literature and Cu/PC800 catalyst with better catalytic performance in this article.

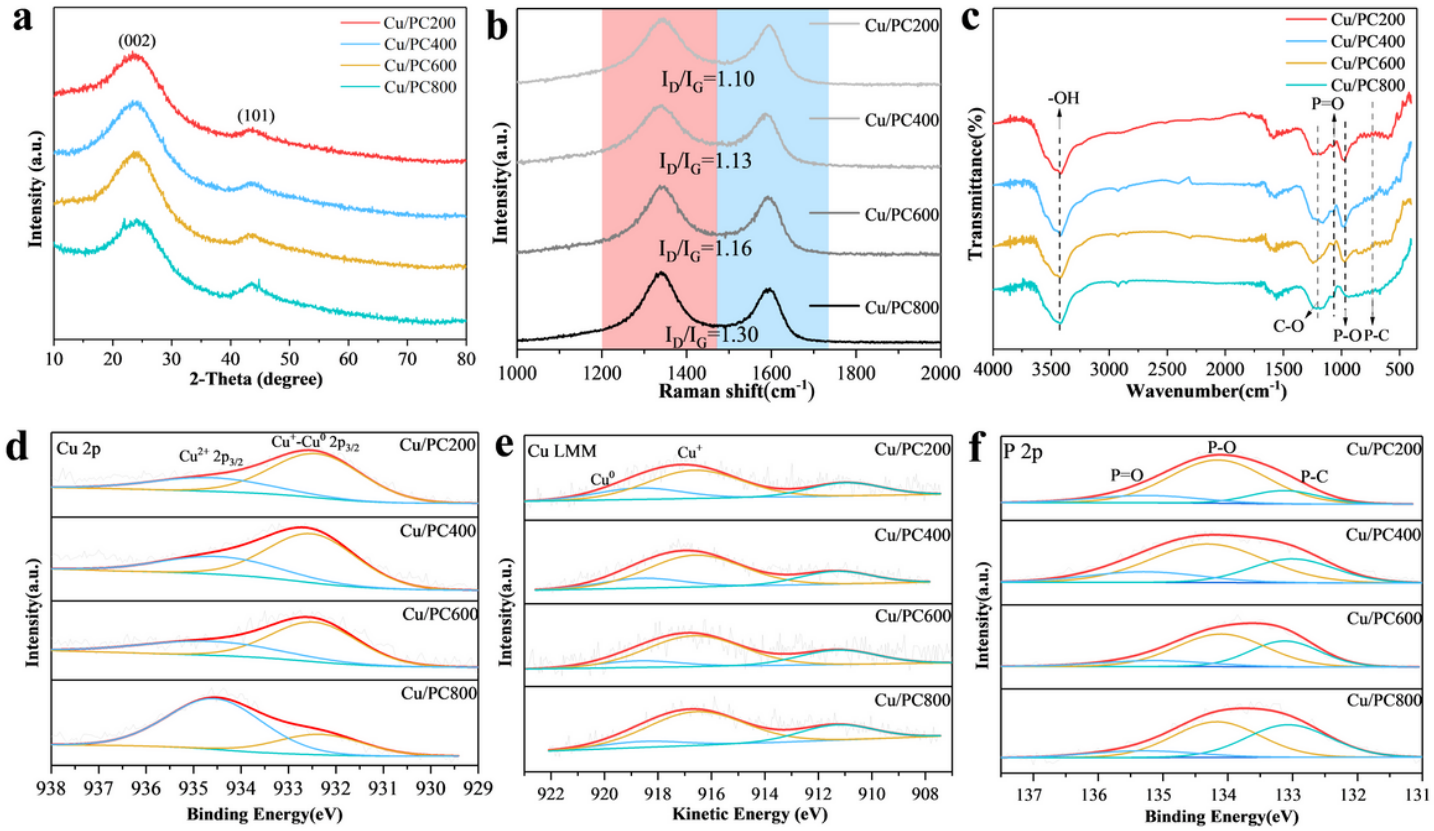

Figure 3

(a) XRD pattern of used P-doped Cu-based catalysts, (b) Raman spectra, (c) FT-IR spectra, (d) Cu 2p XPS spectra and (e) Cu XAES spectra of fresh P-doped Cu-based catalysts, (f) P 2p XPS spectra of fresh P-doped Cu-based catalysts.

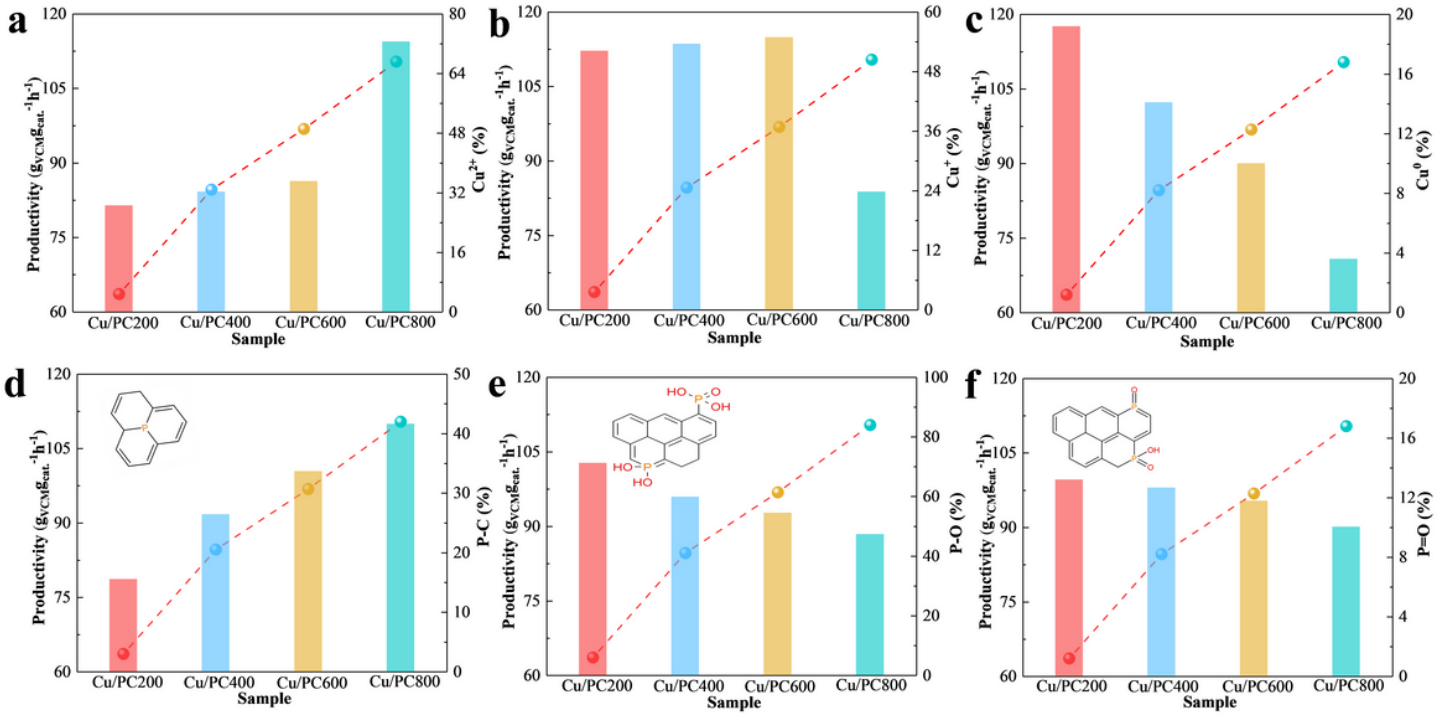

Figure 4

Correlation diagram of (a-c) copper species content, (d-f) phosphorus species content and productivity.

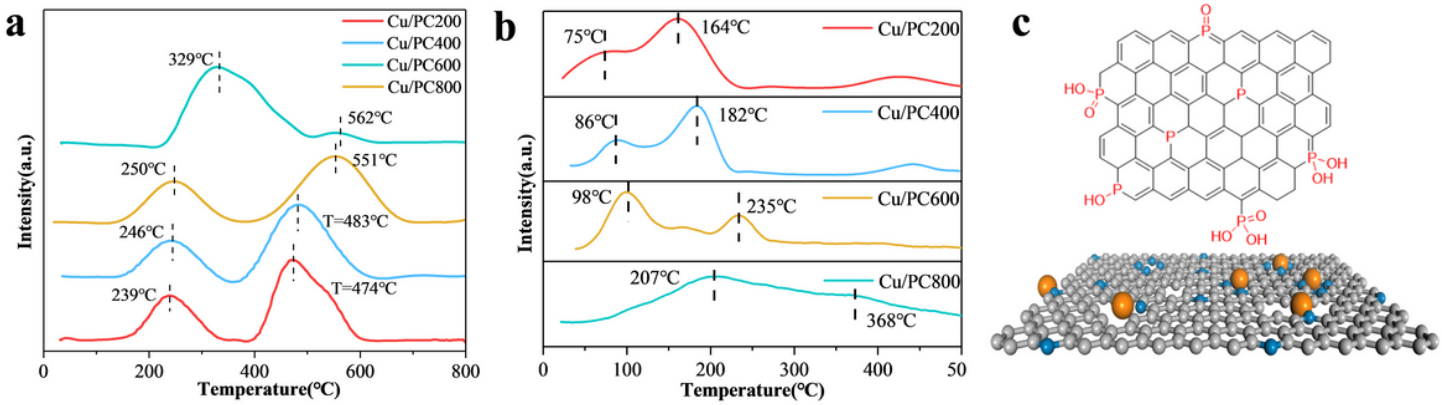

Figure 5

(a) TPR profiles of fresh P-doped Cu-based catalysts, (b) TPD-MS of C2H2 on Cu/PC200, Cu/PC400, Cu/PC600 and Cu/PC800 catalysts, (c) possible structures for P species in fresh P-doped Cu-based catalysts. The gray (carrier), blue and orange balls representing P and Cu atoms.

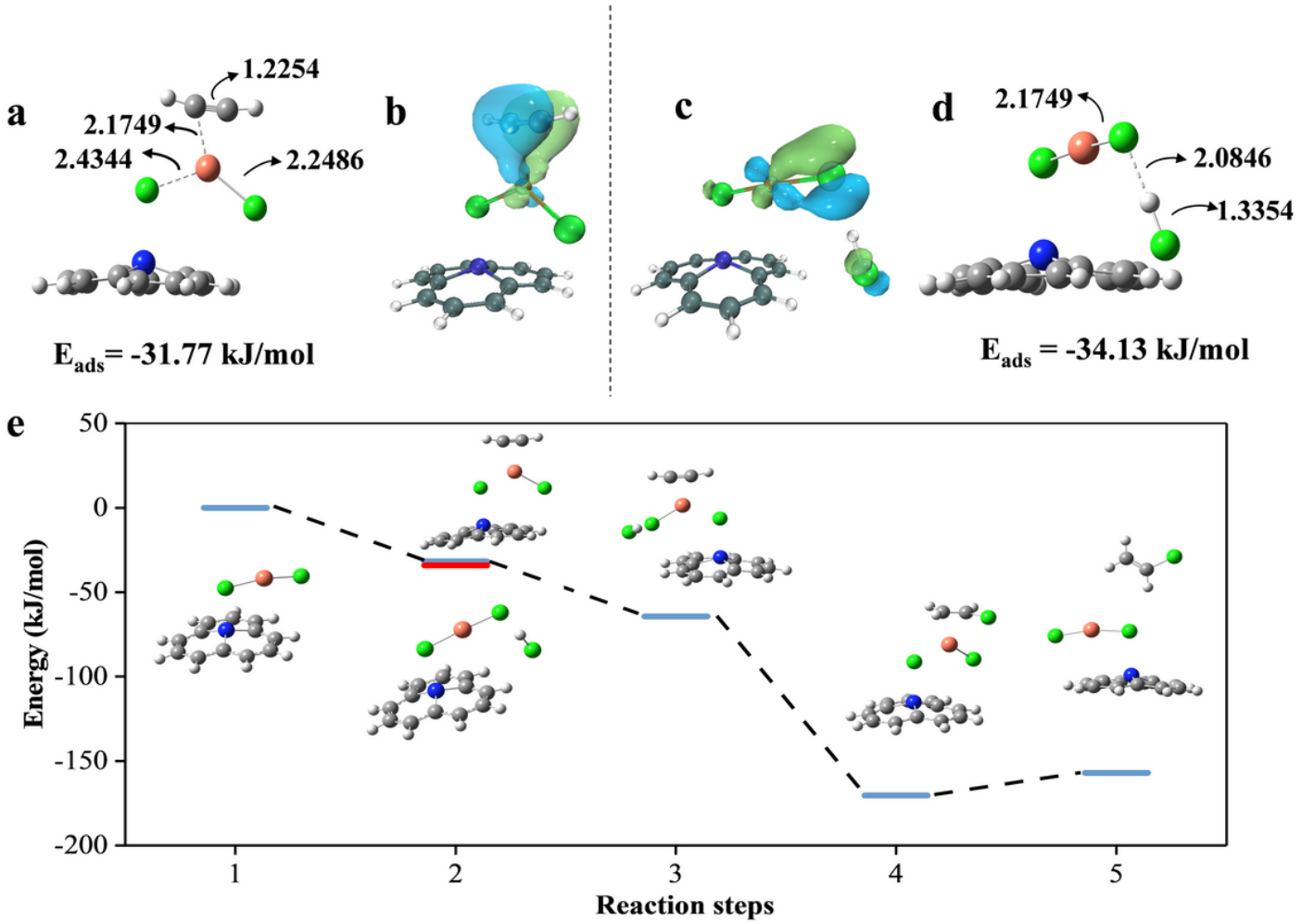

Figure 6

(a) Optimized C2H2 adsorption structure and (d) optimized HCl adsorption structure, the choosed molecular orbital of the (b) C2H2-complex and (c) HCl-complex, (e) Reaction steps of acetylene hydrochlorination on P-doped Cu based catalyst. color scheme: Cu, yellow; C, gray; Cl, green; P, blue; H, white.

Supplementary Files

This is a list of supplementary files associated with this preprint. Click to download.

- IsolatedSingleAtomicCuCatalystSupportedonPdopedCarbonforHydrochlorinationofAcetyleneSI.docx